A Study of Low-Frequency Fluctuations Near the Peru Coast

KENNETH H. BRINK, J. S. ALLEN AND ROBERT L. SMITH

School of Oceanography, Oregon State University, Corvallis 97331

(Manuscript received 22 November 1977, in final form 15 May 1978)

ABSTRACT

An analysis is presented of low-frequency (<0.4 cpd) fluctuations in currents, temperature and tide gage data collected during the March–September 1976 segment of the CUEA JOINT-II experiment off the coast of Peru. The observations were made near 15°S, a region of particularly strong and persistent coastal upwelling. Conclusions about the dynamics of motions over the continental shelf and slope are reached by means of correlations, empirical orthogonal functions and other indicators. It is found that flow over the shelf, where stratification was weak, was generally dominated by vertical turbulent frictional effects and was strongly coupled to the effectively inviscid, baroclinic flow over the slope. The momentum balance was three dimensional, with the alongshore pressure gradient playing an important role. In contrast to behavior in other coastal upwelling regions, the alongshore velocity field over the shelf and slope was evidently not strongly driven by the local alongshore component of the wind stress. The mean wind stress throughout the period was equatorward (upwelling favorable), whereas the mean alongshore currents over the shelf were poleward. The alongshore current fluctuations, which propagated poleward along the coast, were initially poorly correlated with the local wind stress, but during the course of the experiment, the wind stress increased in magnitude and gained in importance as a driving mechanism. The temperature and onshore-offshore current fluctuations over the shelf and, therefore, presumably the upwelling circulation were, however, correlated with the local wind stress throughout the experiment.

1. Introduction

The occurrence of coastal upwelling along the Peru coast under the persistent southeast trade winds and the resulting high biological productivity in the region are well known. Until recently, however, few direct measurements of currents have been made in the Peru coastal upwelling region. Relatively little was known about the mean circulation, or even about variations and the relation of the circulation to the local winds. In contrast, the dynamics of coastal upwelling off Oregon has been interpreted with increasing sophistication using data from moored current meters (e.g., Smith, 1974; Kundu *et al.*, 1975; Kundu and Allen, 1976; Allen and Kundu, 1978). These studies, and other complementary work (e.g., Huyer *et al.*, 1975; Halpern, 1976; Kundu, 1977), resulted from the early field experiments off Oregon by the CUEA (Coastal Upwelling Ecosystems Analysis) program. The culminating CUEA field experiment, called JOINT-II, was off the coast of Peru during 1976–77. The principal aim of this experiment was to better understand the complex physical and biological systems in this upwelling region which was, until the catastrophic warming of the coastal waters (El Niño) during 1972–73, the location of the world's largest fishery.

Although coastal upwelling generally occurs along most of the Peru coast throughout the year, the strongest and most persistent upwelling, as shown by the persistent minimum in sea surface temperatures (Zuta and Urquizo, 1972), occurs between Pisco (14°S) and San Juan (15°20′S). For this reason, the geographical focus of JOINT-II was the continental shelf near 15°S. According to Zuta *et al.* (1975), the upwelling there is maximum in June and August and minimum in December and February. In this paper we investigate the dynamics of upwelling circulation using data from the first part of JOINT-II, which took place during March–October (the Southern Hemisphere fall and winter) 1976. The focus will be on a description of the mesoscale flow field, on the character of the momentum and mass balances and on the driving mechanism(s) for the circulation.

2. The experiment

A number of current meter moorings were deployed along the coast between Callao (12°S) and San Juan (15°20′S) for various intervals during the period 25 March to 30 September 1976. The moorings are indicated in Fig. 1, and the exact positions, depths of instruments and data intervals are given in Table 1[1]. Two primary questions motivated the

[1] The moorings were named after indigenous cacti and succulents except for Sour (near Pisco) and Lagarta.

0022-3670/78/1025-1041$08.50
© 1978 American Meteorological Society

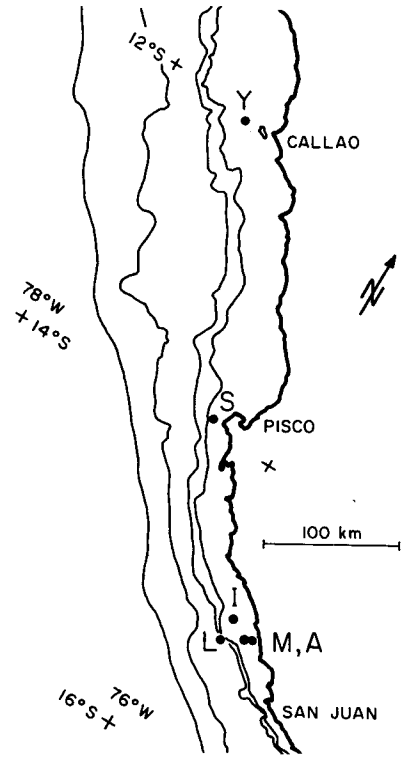

FIG. 1. Locations of current meters during the first three phases of the JOINT-II experiment. The 100, 200, 1000 and 2000 fathom isobaths are shown.

mooring array patterns during the first phase of JOINT-II: What is the variation of the flow regime across the continental shelf and slope? Over what alongshore distances is the flow coherent? For the first question we deployed the L moorings over the inner continental slope, the M moorings at midshelf and the A mooring at the inner shelf. For the second question we deployed a series of moorings at increasing distances equatorward from, but on the same mid-shelf isobath, as the M series moorings. We were able to maintain only the midshelf mooring (Mila) throughout the entire JOINT-II experiment. In the following we treat three periods separately. The periods were determined by the dates of the mooring deployment/recovery cruises, but conveniently represent periods of significantly different wind stress. We refer to these periods (given in Table 1) as Phases I, II and III.

For the current measurements, Aanderaa current meters were suspended on taut moorings beneath subsurface floats at about 20 m; the meters recorded speed, direction and temperature at 20 or 30 min intervals. Hourly data sets were formed and these were filtered to eliminate tidal and higher frequencies by means of a symmetrical low-pass filter (half-power at 0.6 cpd) spanning 121 h. The filter-passed signals have zero amplitude at 1 cpd, half-amplitude at 0.7 cpd and 95% amplitude at 0.5 cpd. The resulting series was then decimated to 6 h

TABLE 1. Measurement locations and dates.

Name	Position (S latitude, W longitude)		Depth (m)	Data interval
	Phase I: March–May 1976			
Agave	15°03′	75°27′	40	25 Mar–6 May
Mila-I	15°05′	75°31′	123	27 Mar–8 May
Lobivia	15°10′	75°39′	656	26 Mar–6 May
Islaya	15°00′	75°39′	136	27 Mar–6 May
Sour	13°55′	76°30′	120	28 Mar–11 May
Sea level (San Juan)	15°21′	75°09′	shore tide gage	from 2 Apr
Sea level (Callao)	12°03′	77°09′	La Punta tide gage	continuous
Wind (San Juan)	15°21′	75°09′	coast	from 25 Mar
	Phase II: May–July 1976			
Mila-II	15°07′	75°30′	128	12 May–26 Jul
Lagarta	15°09′	75°39′	465	11 May–30 Jul
Yuca	12°05′	77°22′	120	15 May–1 Aug
Wind (Callao)	12°03′	77°09′	IMARPE Bldg.	from 21 May
Other wind and sea level data continuous from previous segment				
	Phase III: July–Sept 1976			
Mila-III	15°06′S	75°31′W	123 m	29 Jul–29 Sep
Wind and sea level data continuous from previous segment				

values. The local inertial frequencies are less than 0.52 cpd, so that this component was not entirely removed from the data. However, there was very little inertial signal present in the records. The velocity component spectra rarely show even a weak inertial peak, and the spectral density at the inertial frequency was one or two orders of magnitude lower than in the frequency band 0.05–0.25 cpd. The inertial component was retained because interesting physical effects at nearby frequencies (such as the response to 2–3 day wind fluctuations) would be lost if a "stronger" filter were applied, and because further degrees of freedom would be lost from records that are already short.

Hourly sea level was obtained from coastal tide gages at Callao and San Juan. We estimate the uncertainty in the readings as 3 cm, but filtering the records in the same manner as the current meter data reduces the probable error in the low-passed sea level to 0.5 cm (Mooers and Smith, 1968). Anemometers, located within 1 km of the tide gages and with good exposure to the prevailing coastal wind, recorded winds on a 20 min or continuous basis. The wind data was treated in the same manner as the current meter data.

Hydrographic observations were made at various times throughout JOINT-II. In Fig. 2, two density (σ_t) sections normal to the coast near 15°S, and through the position of Mila, give the hydrographical setting. The first section is from April (Phase I) when moorings (L,M,A) spanned the shelf region; the second section is from August (Phase III) when upwelling is most intense. Both sections show upward sloping isopycnals toward the coast above 70 m indicative of upwelling. The shallowness of the region of upward sloping isopycnals, relative to other coastal upwelling regions, is typical of the Peru region (Wyrtki, 1963; Zuta *et al.*, 1975). The pycnocline at about 70 m is the permanent thermocline, which has an annual average depth of 70 m in this region (Wyrtki, 1964). The 20 m or less mixed-layer depth found during most of the year deepens to about 50 m in midwinter, but a thicker layer of low stratification is often found inshore as a result of upwelling (see Fig. 2a). The deepening of the isopycnals toward the coast below 100 m is consistent with the poleward flow observed over the shelf and upper slope.

The hydrographic features of Fig. 2 are typical of oceanographic conditions usually encountered (cf. Gunther, 1936; Wyrtki, 1963; Zuta *et al.*, 1975). However, along much of the Peru coast during March to August 1976 the sea surface temperature was anomalously warm (Wyrtki, 1977), and the effects on the biota resemble those due to an El Niño event (see *Scientific American*, July 1977, pp. 60 and 62). In the region south of 12°S, and near San Juan in particular, coastal upwelling usually continues unabated during El Niño years. The Mila temperature records show warming from

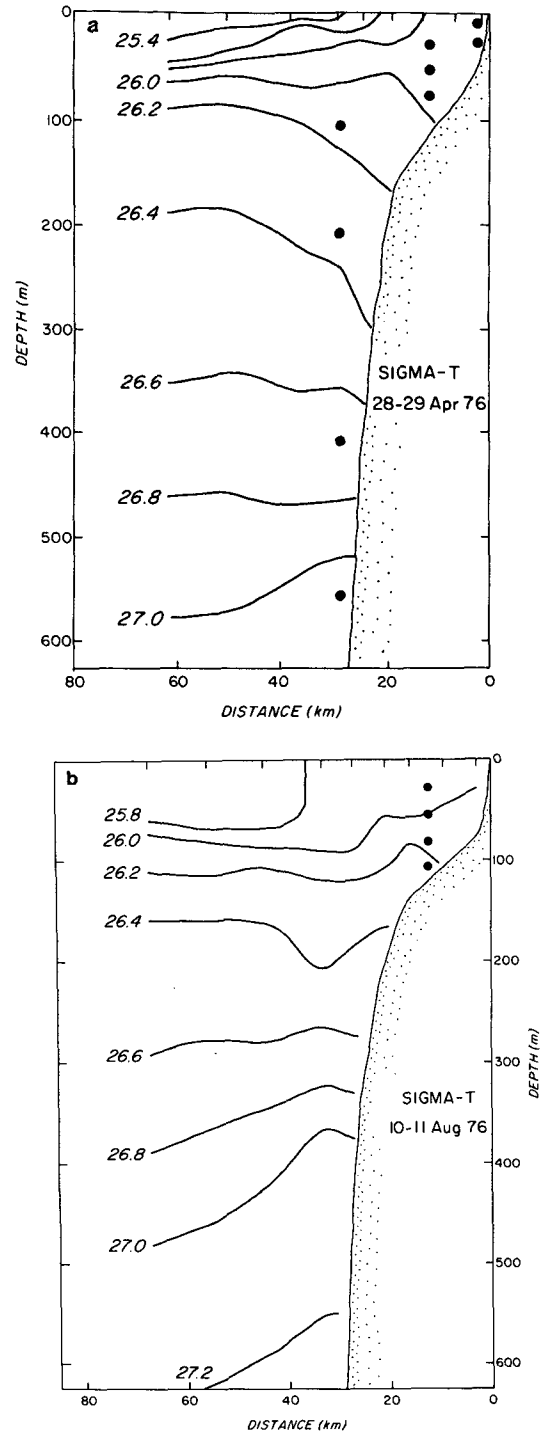

FIG. 2. Vertical sections of sigma-*t* near 15°S. The sections were taken along a line perpendicular to the coast and passing through the Mila mooring. (a) April 1976: Lobivia, Mila I and Agave moorings are shown by large dots; (b) August 1976: Mila III mooring shown by large dots.

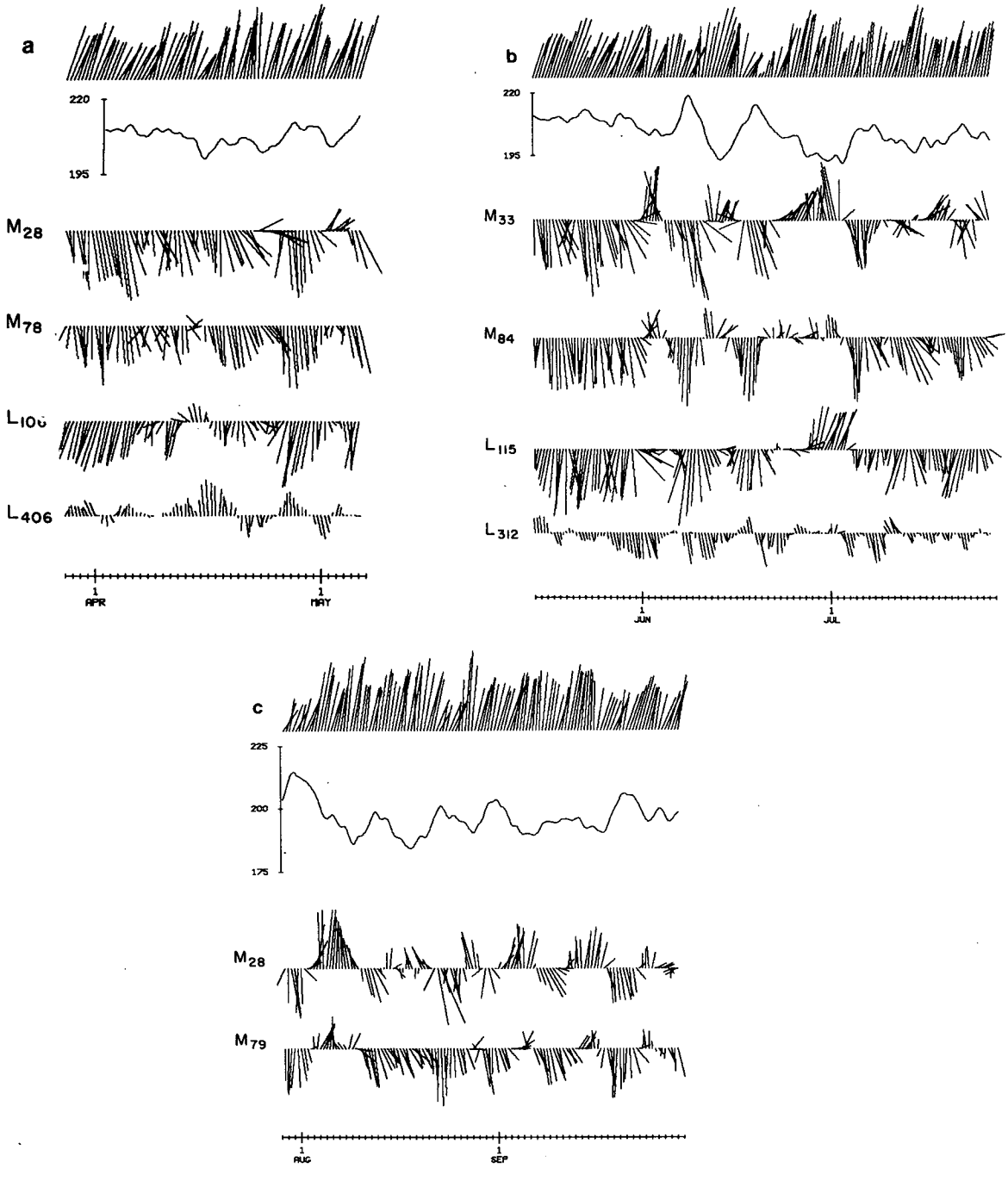

FIG. 3. San Juan wind velocities, San Juan sea level and current meter velocities during the three phases. Scale: 25 cm on the tide gage scale corresponds to 10 m s^{-1} in winds and 50 cm s^{-1} in currents. All currents are rotated into local principal axis system. San Juan winds are rotated 45° toward the northwest. (a) Phase I: wind velocity, sea level and currents at Mila-I 28 and 78 m and at Lobivia 106 and 406 m; (b) phase II: wind velocity, sea level and currents at Mila-II 33 and 84 m and at Lagarta 115 and 312 m; (c) phase III: wind velocity, sea level and currents at Mila-III 28 and 79 m.

the beginning of the records in late March to August—a period when the temperature usually steadily decreases. It is thus possible that the circulation observed during the first phase of JOINT-II is not typical, but is that characteristic of El Niño.

3. General properties of the flow field

Since the coastal topography is not simple, each current meter station is taken to have a local Cartesian coordinate system (x,y) with corresponding velocity components (u,v), where x is positive

TABLE 2. Means, standard deviations and principal axes.

Station	Depth (m)	$\bar{u}$ (cm s^{-1})	$\bar{v}$ (cm s^{-1})	$\bar{T}$ (°C)	u' (cm s^{-1})	v' (cm s^{-1})	T' (°C)	Principal axis directions: θ (deg counter clockwise from N)	Principal axis directions: $\langle\theta\rangle$ (deg counter clockwise from N)	T trend (°C day^{-1})	Mean flow orientation (deg counter-clockwise from N)
a. Phase I: 3/28/76–5/6/76 (39.5 days) $\bar{\tau}^y = 0.82$ dyn cm^{-2} $(\tau^y)' = 0.35$ dyn cm^{-2}											
Agave	10	−0.7	9.8	15.59	6.5	19.4	0.55	28.1	30.5	0.52×10^{-2}	34.6
	29	1.8	−3.5	15.12	3.6	13.3	0.43	32.8		0.65×10^{-2}	237.7
Sour	80	1.8	−25.2	14.69	3.9	14.4	0.36	23.9	21.8	0.53×10^{-2}	205.9
	100	−1.1	−19.2	14.47	2.6	12.3	0.37	19.7		0.44×10^{-2}	198.5
Lobivia	106	−3.0	−15.3	13.77	4.1	12.4	0.36	52.2	61.6	0.61×10^{-2}	240.5
	206	0.0	−1.9	13.00	3.4	15.2	0.19	53.0		0.08×10^{-2}	241.6
	406	0.0	3.1	10.33	1.4	8.0	0.75	66.1		-0.67×10^{-2}	61.6
	556	0.1	−0.8	7.39	2.1	4.0	0.26	41.3		-0.15×10^{-2}	234.5
	626	−1.1	−0.4	6.58	2.6	1.9	0.23	95.3		-0.11×10^{-2}	171.6
Islaya	41	6.5	−19.4	15.12	8.4	12.8	0.55	37.6	30.9	1.15×10^{-2}	229.4
	66	3.9	−19.7	14.55	5.3	10.2	0.41	31.1		0.88×10^{-2}	222.1
	116	−1.1	−13.4	14.10	3.3	10.2	0.35	23.9		0.54×10^{-2}	206.2
Mila I	28	6.3	−19.9	15.50	6.3	13.6	0.56	27.2	38.9	1.05×10^{-2}	236.5
	53	3.6	−22.6	14.65	4.6	9.5	0.41	42.1		0.88×10^{-2}	228.0
	78	2.3	−19.0	14.36	4.2	9.3	0.37	47.4		0.65×10^{-2}	225.8
b. Phase II: 5/15/76–7/26/76 (72.25 days) $\bar{\tau}^y = 0.86$ dyn cm^{-2} $(\tau^y)' = 0.45$ dyn cm^{-2}											
Yuca	80	3.2	−14.2	16.92	5.2	16.1	0.37	23.3	23.3	-0.26×10^{-2}	216.0
Lagarta	115	1.0	−16.9	14.58	7.1	19.7	0.48	45.1	57.1	0.04×10^{-2}	240.5
	212	0.3	−8.9	12.87	2.9	11.8	0.40	59.0		-0.17×10^{-2}	239.0
	312	0.8	−5.5	11.63	2.1	9.0	0.35	66.9		-0.21×10^{-2}	245.4
	412	−0.2	+0.1	9.81	1.0	5.0	0.49	57.4		-0.34×10^{-2}	120.5
Mila II	33	4.5	−8.1	16.75	7.8	25.6	0.48	45.5	41.7	0.15×10^{-2}	250.8
	62	4.7	−14.9	15.91	5.4	21.8	0.65	41.1		0.27×10^{-2}	239.2
	84	2.6	−16.1	15.36	5.4	19.1	0.59	42.6		0.13×10^{-2}	230.9
	109	0.3	−9.9	14.90	3.7	14.2	0.57	37.9		0.03×10^{-2}	223.4
c. Phase III: 7/29/76–9/29/76 (62 days) $\bar{\tau}^y = 1.05$ dyn cm^{-2} $(\tau^y)' = 0.52$ dyn cm^{-2}											
Mila III	28	2.4	2.9	14.87	5.3	21.6	0.59	48.5	44.6	-0.37×10^{-2}	5.0
	53	7.9	−5.7	14.76	4.5	18.8	0.57	46.1		-1.27×10^{-2}	278.8
	79	3.8	−11.1	13.65	4.3	15.8	0.64	44.1		-1.11×10^{-2}	243.5
	104	0.5	−8.2	13.30	4.5	12.3	0.67	39.7		-0.99×10^{-2}	228.1

toward the shallower water (northeast) and y is positive alongshore toward the northwest. Each system is defined by the depth-averaged principal axis direction $\langle\theta\rangle$ of the current meter records. The physical justification is that low-frequency fluctuations on a continental shelf tend to be along the local isobaths (Kundu and Allen, 1976; Allen, 1976). Since knowledge of the local bathymetry is limited, the principal axis coordinate system shall be used even though frictional effects and stratification can cause a rotation of the principal axes relative to the local topography. Fig. 3 shows stick diagram plots of wind stress and selected current meter records. The San Juan wind data was rotated 45° toward the northwest, parallel to the local coast line.

The means (denoted by overbars), standard deviations (denoted by a prime) and principal axis directions θ (measured counterclockwise from true north) are presented in Table 2, along with the means and standard deviations of the alongshore component of wind stress as measured at San Juan, about 55 km southeast of the Mila station. Tempera-

ture can be taken as an accurate indication of the behavior of the density field, since in this region σ_t and T are highly correlated and T largely determines the σ_t behavior (Barton, 1977). Means are taken over the common record length of each phase.

Perhaps the most striking feature about the flow is that although the mean wind stress is toward the northwest, the alongshore component of mean flow is generally in the opposite sense. This phenomenon differs from that in the other major upwelling areas studied by the CUEA program, Oregon and northwest Africa (Kundu and Allen, 1976; Mittelstaedt, *et al.*, 1975), although it was observed before off Peru (Smith *et al.*, 1971). This southeastward flow may be related to a shoaling of the Peru-Chile Undercurrent or to a displacement of the Peru Countercurrent (Wyrtki, 1963). During Phase I, only at Agave at 10 m,[2] which is clearly in the mean surface mixed layer, and at Lobivia 406, which represents a weak current opposite to the shallow currents, is the mean flow in the direction of the mean wind. As the experiment progressed, the mean southward alongshore velocities on the shelf became weaker while the northward wind stress became stronger. During Phase III, $\bar{v}$ at the shallowest Mila current meter (28 m) was in the same sense as the wind stress.

The mean $\bar{u}$ velocities indicate a net onshore flow throughout the experiment with weak offshore (negative) flow in the surface mixed layer (Agave 10) and near the bottom on the shelf (Sour 100, Islaya 116) during Phase I. The decrease in $\bar{u}$ at Mila III (28 m) relative to the earlier values at that position seems to indicate a deepening of the mean surface mixed layer in which the flow is expected to be generally offshore.

The mean temperatures are difficult to interpret because of slight variations in the measurement depths. The difference in $\bar{T}$ between Yuca at 80 m (16.92°C) and Mila II at 84 m (15.20°C) is significant, however. In fact, the water at 80 m at Yuca is warmer than that at 33 m depth at Mila II. There must then exist an alongshore temperature gradient on the shelf of the order of 5×10^{-3}°C km^{-1}. This means that the mean flow along the shelf effects a poleward advective heat flux, and suggests that there is a mean alongshore baroclinic pressure gradient associated with the mean onshore flow. The alongshore density gradient implies a negative mean vertical shear in $\bar{u}$ consistent with the observations at Islaya, although bottom friction may also be a factor at that mooring. A similar temperature difference is also evident in comparing mean temperature at Sour 80 and Mila I 78.

[2] Hereafter often referred to simply as Agave 10.

Table 2 also shows the linear trends in temperature (which were removed from the data during subsequent analyses). The earliest phase shows warming at all of the shallower current meters, opposite to what one might expect during the Southern Hemisphere autumn. This tendency is probably due to the 1976 El Niño event. During Phase II (May–July) the warming continues but not nearly as strongly (cf. Mila temperature trends). During Phase III (July–September) there is a trend of decreasing temperature, which reflects a strong cooling (~1.5°C) on about 4 August. Even though there is a warming in the shallower waters during Phases I and II, the deeper waters over the slope have a trend of decreasing temperature.

Standard deviations of the onshore flow are almost invariably greater than means throughout the experiment. This is a reflection of the weakness of the mean onshore flow. During Phase I the standard deviations of v are smaller than the means on the shelf, reflecting the predominantly southward flow. Finally, one can note the unusually large temperature standard deviation of 0.75°C at Lobivia 406, reflecting isotherm displacements in a region of relatively large vertical temperature gradient (see Fig. 2).

Correlations between u records are generally only significant at 95%[3] for pairings of records from the same mooring, and are poor otherwise. This appears to reflect the dominance of "turbulence" over the u signal, as suggested by Kundu and Allen (1976) for similar results off the Oregon coast.

Correlations in v, being quite a bit larger than those in u, suggest that the signal in v is stronger than the "turbulent" noise. Of particular interest are the strong correlations, visible in Fig. 3, between v from shallow slope records (Lobivia 106 and Lagarta 115) and v from the shelf time series. This suggests that roughly the upper 125 m of the water column moves coherently alongshore, regardless of total depth. Distances over which correlations in v are significant are quite long relative to those for u. At any one mooring on the shelf, the v records are significantly intercorrelated over the total depth range (~100 m). Correlations of v along and across the shelf remain fairly high and significant at alongshore separations up to about 170 km, the distance between Mila and Sour.

Temperature correlations, although sometimes numerically high, are often not significant at the 95% level because the relative absence of high-frequency signal gives them broad autocorrelation functions, hence few degrees of freedom. Significant

[3] The number of degrees of freedom for each correlation is found using the technique employed by Davis (1976).

temperature correlations generally occur only between different depths at the same station. An exception to this rule is the high correlations (ranging from 0.46 to 0.69) between the Lagarta 115 record and the records at Mila II, which again emphasizes the strong onshore-offshore coupling in the shallower waters already mentioned with respect to the v correlations.

4. Physical properties of the flow field

In this section, empirical modal decompositions (Kundu *et al.*, 1975; Kundu and Allen, 1976) are used to describe the structural characteristics and some dynamical properties of the fluctuations.

Table 3 presents the two most energetic empirical orthogonal modes of u, v and T at each mooring (except Yuca, where only one current meter operated successfully), along with the percent of total variance for which the mode accounts. The modes are denoted by ϕ_n^q associated with the amplitude time series E_n^q, where q is the variable in question (u, v or T) and n the mode number. Modes are ordered by variance, i.e., the first mode is the most energetic, etc. The modes are orthonormal such that

$$\sum_{j=1}^{M} \phi_n(z_j)\phi_m(z_j) = \delta_{nm}, \tag{4.1}$$

where M is the number of current meters in the mooring, z_j are the depths of the instruments and δ_{nm} is the Kronecker delta. The first modes generally account for about 75% or more of the energy, except for some u modes and a few T modes. The u modes are expected to have a lower "signal-to-noise" ratio, because of "turbulence". The two cases where temperature is most poorly represented by the first mode (Islaya and Mila I) are both shelf moorings and seem to represent cases where mixing and advection are of comparable importance in influencing time variations of the density structure. In all cases the first alongshore velocity modes ϕ_1^v possess significant depth dependence. The modes from shelf moorings do not have zero crossings, while those over the slope either have a zero crossing or closely approach one. The first modes of temperature at the slope moorings are dominated by the signals at about 400 m, consistent with depth fluctuations of the relatively strong vertical temperature gradient (~2°C in 80 m) at about that depth (see Fig. 2). Below the level of this strong gradient, motions are noticeably weaker, so that 400 m density fluctuations seem to partially compensate for shallower pressure gradients.

a. Baroclinicity

It is desirable to know how well the alongshore flow at a given mooring is governed by effectively inviscid baroclinic dynamics, e.g., how well the thermal wind equation holds. If the fluctuations are baroclinic for a geostrophically balanced alongshore flow, then the isotherms, representing isopycnals, should be locally fluctuating in a manner correlated in some sense with the local alongshore flow. Even though v and the cross-shelf gradient of T must be highly correlated, it is not necessary that v and T at the same location be correlated nor that the vertical density structure at one location be correlated with the velocity field (consider the special case of the center of a two-layer channel flow, which is baroclinic, but where the interface height remains at its static position). A tentative measure of the degree of baroclinicity can be obtained by considering an empirical mode of both v and T, i.e., ϕ^{vT}. The velocities are normalized to unity total variance, as are the temperatures, to give the two equal *a priori* weights. This procedure was applied by Wang and Walsh (1976) in a different problem involving modes of mixed quantities. Since the various empirical modes of a given set of records are uncorrelated, one expects that if the v and T fields are uncorrelated, the ϕ^{vT} modes will segregate into modes that represent velocity and temperature separately. On the other hand, if the flow is baroclinic so that the v and T fields are coupled, one might expect to see each ϕ^{vT} mode represent roughly equal contributions from each field, although this does not have to be true for every mode. Table 4 displays some of the ϕ^{vT} modes. The deeper slope mooring, Lobivia, has nearly equal weights in each mode from v and T, suggesting that the fluctuations there are baroclinic, consistent with more qualitative observations based on the separate modal structure. Lagarta, a shallower slope mooring, seems to represent an intermediate case, while the Mila records from Phase I and II separate so strongly as to suggest a nonbaroclinic balance. However, the first ϕ^{vT} mode computed for Mila III suggests baroclinic dynamics. Estimates of kinetic ($\frac{1}{2}\rho v'^2$) and potential $[\frac{1}{2}(g/\rho_0)(\partial\bar{T}/\partial z)^{-1}T'^2]$ energy at these locations, using current meter velocity and temperature records, show that for all reported cases, the net energy of both forms is of the same order. There is no pattern in energy distributions that indicates the baroclinicity or nonbaroclinicity that the modes suggest.

The individual velocity and temperature time series also indicate that the density and momentum fields are strongly coupled over the slope. A particularly dramatic example is displayed in Fig. 4, where the time series of T at Lobivia 406 is plotted along with alongshore velocity v of Lobivia 206. The two records are strongly correlated (−0.81 at zero lag), consistent with a thermal wind balance

TABLE 3. Empirical orthogonal functions.

		u modes		v modes		T modes	
		ϕ_1^u	ϕ_2^u	ϕ_1^v	ϕ_2^v	ϕ_1^T	ϕ_2^T
				Phase I			
Agave	Percent variance	79.9	20.1	92.3	7.7	94.2	5.8
	(E,τ^v)	0.22	0.34*	−0.02	−0.18	0.06	0.37*
	10 m	−0.97	0.24	−0.84	−0.53	−0.80	−0.61
	29 m	0.24	0.97	−0.53	0.84	−0.61	0.80
Sour	Percent variance	74.1	25.9	97.3	2.7	93.8	6.2
	(E,τ^v)	0.02	−0.04	0.20	0.35	0.04	0.21
	80 m	−0.96	−0.29	−0.76	−0.65	0.67	−0.74
	100 m	−0.29	0.96	−0.65	0.76	0.74	0.67
Lobivia	Percent variance	47.4	24.0	75.7	14.8	76.5	11.6
	(E,τ^v)	−0.01	0.12	0.32*	0.07	−0.10	−0.11
	106 m	−0.86	0.34	−0.61	−0.39	0.34	−0.45
	206 m	−0.50	−0.63	−0.79	0.20	−0.03	−0.44
	406 m	−0.07	0.15	−0.09	0.90	−0.93	−0.07
	556 m	0.02	−0.33	−0.01	−0.01	−0.15	−0.56
	626 m	0.01	−0.60	−0.01	−0.02	0.03	−0.53
Islaya	Percent variance	76.6	18.8	86.4	11.1	48.8	43.2
	(E,τ^v)	−0.11	0.38	0.16	0.04	−0.44*	−0.24
	41 m	−0.90	−0.44	−0.68	0.52	0.80	0.49
	66 m	−0.44	−0.89	−0.55	0.10	−0.05	0.63
	116 m	−0.03	0.10	−0.48	−0.85	−0.60	0.60
Mila I	Percent variance	68.9	19.7	87.3	10.8	56.8	39.5
	(E,τ^v)	−0.34	0.23	0.23	−0.15	0.45*	−0.05
	28 m	−0.79	−0.61	−0.73	−0.67	−0.96	0.25
	53 m	−0.47	0.60	−0.51	0.36	−0.25	−0.56
	78 m	−0.40	0.51	−0.46	0.65	−0.12	−0.79
				Phase II			
Lagarta	Percent variance	78.6	14.4	74.4	16.3	57.7	21.9
	(E,τ^v)	0.22	−0.04	−0.16	−0.24	0.14	0.14
	115 m	1.00	−0.08	−0.89	0.33	−0.52	0.83
	212 m	0.07	0.91	−0.45	−0.47	−0.47	−0.15
	312 m	0.04	0.40	0.11	−0.79	−0.37	−0.39
	412 m	0.00	−0.02	0.01	−0.23	−0.60	−0.37
Mila II	Percent variance	54.0	30.3	92.4	6.1	78.8	17.3
	(E,τ^v)	0.05	0.63*	−0.26	−0.08	0.00	−0.15
	33 m	−0.86	−0.42	−0.63	−0.57	−0.64	−0.61
	62 m	−0.45	0.41	−0.54	−0.13	−0.52	−0.05
	84 m	−0.18	0.76	−0.46	0.50	−0.45	0.40
	109 m	−0.14	0.27	−0.32	0.64	−0.35	0.68
				Phase III			
Mila III	Percent variance	41.1	38.5	94.2	3.9	89.6	7.6
	(E,τ^v)	0.36*	0.63*	−0.46*	−0.21	0.49*	−0.26
	28 m	0.28	−0.83	−0.62	−0.56	−0.44	−0.81
	53 m	0.55	−0.27	−0.55	−0.16	−0.47	−0.15
	79 m	0.54	0.38	−0.45	0.48	−0.53	0.29
	104 m	0.57	0.31	−0.33	0.66	−0.55	0.50

* Correlations significant at 95%.

in a coastal trapped motion. The high correlation of the two records is reflected in the structure of the ϕ^{vT} mode (see Table 4).

b. *Bottom friction*

On the shelf, the velocity fluctuations appear nonbaroclinic (except for Mila III), yet still have significant depth-dependence in the most energetic modes. The explanation appears to involve the importance of the turbulent bottom boundary layer on the shelf. Although we have no direct proof of this, some reasonable arguments exist.

First, the depth of the bottom logarithmic and turbulent Ekman layers may be calculated using the formulas presented by Wimbush and Munk

TABLE 4. Empirical modes of v and T: ϕ^{vT}.

	Mila I			Lobivia	
	ϕ_1^{vT}	ϕ_2^{vT}		ϕ_1^{vT}	ϕ_2^{vT}
percent variance	50.8	25.5	percent variance	71.6	11.9
T part of (norm)^2	0.20	0.93	T part of (norm)^2	0.50	0.52
v part of (norm)^2	0.80	0.07	v part of (norm)^2	0.50	0.48
T 28 m	−0.44	−0.66	T 106 m	−0.15	0.46
53 m	0.02	−0.50	206 m	0.07	0.36
78 m	0.09	−0.50	406 m	0.68	−0.28
v 28 m	−0.63	0.20	556 m	0.13	0.18
53 m	−0.46	0.14	626 m	−0.03	0.27
78 m	−0.43	0.09	v 106 m	−0.40	−0.58
			206 m	−0.57	−0.03
			406 m	−0.09	0.36
			556 m	0.00	−0.07
			626 m	−0.01	−0.03

(1970). These state that the Ekman layer depth is given by

$$\delta_{EK} \approx 0.4 u_* f^{-1}, \tag{4.2}$$

the log layer depth by

$$\delta_{ln} \approx 2 u_*^2 f^{-1} V_g^{-1}, \tag{4.3}$$

and the friction velocity by

$$u_* \approx 0.04 V_g, \tag{4.4}$$

where V_g is the geostrophically balanced flow immediately above the frictional layer and f the local Coriolis parameter. The depths calculated based on the mean alongshore flows at Mila are presented in Table 5. These values appear reasonable, since Kundu (1977) has shown that the formulas are consistent approximations off northwest Africa, where the stratification is as weak as it is on the Peru shelf ($\bar{\rho}_z \approx 0.5 \times 10^{-7}$ g cm^{-4} in both cases). Since the depth at Mila is about 123 m, it is clear that the local turbulent bottom Ekman number (the ratio of Ekman layer depth to total fluid depth) remains order 1 throughout the experiment, although it does decrease by a factor of about 2. The importance of bottom friction can explain the large shears observed in the nonbaroclinic shelf flow.

A second piece of evidence supporting the importance of bottom friction is less direct. Brink and Allen (1978) have demonstrated that the presence of friction on a continental shelf can give rise to cross-shelf phase lags such that nearshore events lead those offshore by a time proportional to the cross-shelf gradient of the local Ekman number. This prediction is verified qualitatively by the cross-shelf maximum lagged correlations presented in Table 6. This agreement strengthens our belief in the importance of friction.

Further evidence of bottom friction is the rotation of the mean velocities with depth (Table 2). The vectors in the lower part of the water column over the shelf rotate clockwise with increasing depth, consistent with the Southern Hemisphere Ekman spiral. The same sense of rotation is present in the principal axis directions from current meters sufficiently close to the bottom [e.g., Islaya (41 m, 66 m, 116 m), Mila II (84 m, 109 m) and Mila III (28 m, 53 m, 79 m, 104 m)].

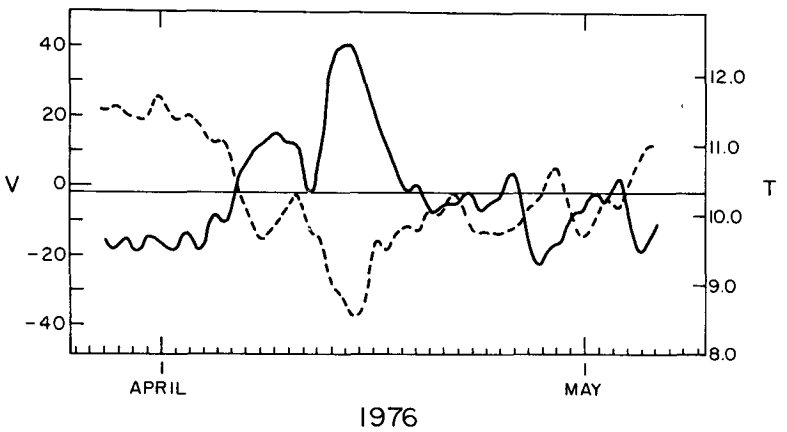

FIG. 4. Alongshore velocity (solid line) at 206 m and temperature (dashed line) at 406 m, both from the Lobivia mooring over the continental slope.

TABLE 5. Bottom frictional layer depths at Mila.

	δ_{1n} (m)	δ_{EK} (m)	u_* (cm s^{-1})
Mila I	16–24	80–120	0.8–1.1
Mila II	13	60	0.6
Mila III	5–9	24–47	0.2–0.4

c. *Momentum equation balances*

As a means of understanding more about the detailed momentum balances, a study similar to that in Allen and Kundu (1978) was made. The usual approximate momentum equations for low-frequency motions over a continental shelf-slope system (Allen and Kundu, 1978) are

$$\rho(v_t + fu) = -p_y, \tag{4.5}$$

$$\rho fv = p_x, \tag{4.6}$$

where f is the Coriolis parameter (-3.76×10^{-5} s^{-1} at 15°S), ρ the density and p the pressure. Subscripts x, y, t represent partial differentiation. Terms involving velocities were calculated using current meter data. Time derivatives were obtained by finite differencing with Δt = 12 h. Data on total pressure gradients were unavailable but the existence of tide gage records at San Juan (~15°20′S) and Callao (~12°S) allowed the calculation of a surface alongshore pressure gradient at the coast, $\rho g \zeta_y = P_y$, where ζ is the free surface displacement positive upward and $P = g\rho\zeta$. Insufficient atmospheric pressure data were available to calculate a "subsurface" pressure (atmospheric plus sea level), but enough data (about two months overlapping Callao tide gage and San Martin atmospheric pressure at 14°S) did exist to evaluate the importance of this correction. Sea level fluctuations were more energetic than atmospheric pressure fluctuations (standard deviations of sea level, atmospheric pressure and "subsurface" pressure are 2.8, 1.3 and 2.8 cm, respectively), and a low correlation (−0.28) between sea level and atmospheric pressure was found. The uncorrected sea level is highly correlated (0.85) with corrected sea level. With this in mind, we feel that it is valid to compare currents with uncorrected sea level. In taking the alongshore pressure derivative, correction for atmospheric pressure is unimportant as long as the distance between tide gages (~435 km) is small relative to the scale of atmospheric pressure fluctuations. Analysis of 1977 atmospheric pressure data from along the Peru coast indicates that fluctuations are virtually constant over an alongshore scale of about 600 km (H. Pittock, personal communication).

Table 7 presents correlations between approximated terms in the momentum equations. The correlations relevant to the alongshore momentum equation (4.5) indicate that the strongest balance is between the alongshore pressure gradient P_y and v_t. The correlations between v_t and fu and between fu and P_y are markedly lower. "Turbulence" or other effects in u may be masking the component related to v_t and P_y, thus lowering their correlations with fu. Fig. 5 displays sample time series of v_t, fu and P_y. Table 8 presents standard deviations of the quantities indicating that the magnitudes of all three terms are indeed comparable. The (v_t,P_y) correlations fall off with depth at Lobivia and Lagarta as expected for a case with baroclinic flow which is weak at depth, and where there is "noise" which does not decrease as quickly with depth. The only other nonsignificant (v_t,P_y) correlation appears at Yuca, off Callao, which is at one end of the finite-difference interval, so the calculated P_y would not be as relevant there. The balance of v_t and P_y is suggestive of a free Kelvin wave. The external form seems unlikely because the alongshore propagation speeds observed by Smith (1978) of about 200 km day^{-1} do not agree with the barotropic Kelvin wave speed of the order of thousands of kilometers per day. The motions are apparently baroclinic and could represent internal Kelvin waves or more general baroclinic coastal trapped waves (Allen, 1975; Wang and Mooers, 1976). The weak velocities at depth make a pure barotropic shelf wave seem unlikely.

Table 3c shows that the first empirical mode of u at Mila III has little depth variation below the upper current meter (which is probably influenced by the surface layer), a structure consistent with a barotropic model. Since the u mode structure is consistent with a recognizable dynamical pattern, we expect that in this case the mode may have isolated the u component which contains no "turbulence". If this were true, the (v_t,fu) correlation should be improved over the pointwise cases where turbulence is not removed. As a test, $(E_1^v)_t$ and fE_1^u were compared at Mila III and the correlation was −0.43, a value notably better than the highest Mila III

TABLE 6. Cross-shelf lagged correlations.

Nearshore record	Offshore record	Zero-lag correlation	Maximum lagged† correlation (lag in days)
Agave E_1^v	Mila I E_1^v	0.48*	0.66* (1.0)
Agave 29 v	Mila I 28 v	0.52*	0.69* (1.0)
Agave 29 v	Mila I 53 v	0.44*	0.58* (1.0)
Mila II 84 u	Lagarta 115 u	0.23*	0.40* (0.25)
Mila II 84 v	Lagarta 115 v	0.77*	0.78* (0.25)

* Correlation valid at 95%.

† The nearshore record leads offshore in all cases.

pointwise (v_t,fu) correlation of -0.34. Thus, it seems that E_1^u at Mila III represents a nearly barotropic component of u which obeys to some extent the dynamics included in (4.5).

The x momentum equation (4.6) states that geostrophic balance exists for the alongshore flow. This is partially based on the assumption that u_t is small relative to fv, which is generally confirmed by the results in Table 8. However, u_t is not as small relative to fv as was found off Oregon (Allen and Kundu, 1978). If v is geostrophically balanced and if only coastal trapped motions exist, then v and P should be correlated. Table 7 shows the correlations between P (not corrected with atmospheric pressure) and v. The lagged correlations are the relevant quantities because the current meters are far enough from the tide gages that propagation effects must be accounted for. It can be seen that the (v,P) correlations are generally large and negative, as expected for geostrophic balance. The correlations fall off with depth at Lobivia, Lagarta and Mila III, consistent with the baroclinic behavior predicted from the ϕ^{vT} modes and with the arguments presented above in connection with the decrease in (v_t,P_y) correlations. The decrease is probably not explained by bottom frictional effects in this case because friction would enter (4.6) through u, which is small relative to v. It seems reasonable to conclude that the alongshore flow is basically in geostrophic balance and that baroclinic effects and "turbulence" account for (v,P) correlations of less than unity.

The alongshore momentum balance (4.5) remains puzzling. The standard deviations of $(v_t + fu)$ and P_y are of the same order, but the variables are not highly correlated, suggesting there may be other terms in the balance. This conclusion must be somewhat tempered by the fact that the calculated P_y is not a good estimate because of the noisiness of the tide gage records, and the long differencing interval. The baroclinic pressure gradient must be of some importance, as are probably turbulent frictional effects. Nonlinear effects are also a possibility, since a Rossby number $\mathrm{Ro} = v(fL)^{-1} = (15\ \mathrm{cm\ s^{-1}}) \times (3.76 \times 10^{-5}\ \mathrm{s^{-1}} \times 20\ \mathrm{km})^{-1} \approx 0.25$ is not really small.

d. First-order wave equation

The high (v_t,p_y) and (v,P) correlations suggest that the alongshore momentum balance is three-dimensional and the alongshore velocity is in geostrophic balance. The three-dimensionality of the flow is supported by Smith's (1978) result, obtained by lagged correlations of velocities, that disturbances propagate southward along the shelf at a rate of about 200 km day^{-1}. Regardless of its detailed form, if there is a low-frequency long coastal trapped wave, it will be governed by (Clarke, 1977)

$$-c_n^{-1}\phi_{nt} + \phi_{ny} = b_n\tau^y, \tag{4.7}$$

where friction is ignored, $\phi_n(y,t)$ gives the alongshore and time-dependent behavior of cross-shelf mode number n, c_n is that mode's phase speed and b_n a coupling coefficient with the wind stress.

With the hypothesis that the motion is dominated by one mode (i.e., one value of n) we attempted to check the validity of (4.7) by using P to represent ϕ_n. Sea level records of length 256 days from Callao and San Juan, which are about 435 km apart (atmospheric pressure was unavailable), were used. P_t was computed by finite differencing (Δt = 12 h) the record of the average of the two sea level records. The attempt proved unsuccessful because of the weak (0.25) correlation between P_t and P_y, although this value is significant at the 95% level and has the proper sign for a southward propagating disturbance. Phase speeds obtained by a regression analysis using P_t and P_y were either 55 or 880 km day^{-1}, depending on which way the regression was performed. The scatter in the values of c_n using different regression techniques is a consequence of the low (P_t,P_y) correlation. The results were not improved by the use of multivariate regression including the wind stress and a frictional term in (4.7). The speed calculated by balancing of the standard deviations of $(c^{-1}P_t)$ and P_y [equal to the geometric mean of the two regression values and derived by minimizing the sum of squared deviations with respect to $(c_n^2 \sum P_y^2 + \sum P_t^2)$] is 224 km day^{-1}. This is in reasonable agreement with Smith's (1978) values. The low correlation of P_t and P_y is probably due in part to large measurement errors in ζ (~0.5 cm after filtering) and to finite-difference errors.

R. C. Beardsley (personal communication) pointed out that because of finite-difference errors in P_y, this technique should be more accurate for wavelengths which are large compared to the separation L (435 km) between tide gages, i.e., for periods larger than $L\,c_n^{-1}$ (~2 days), assuming nondispersive waves. The data were therefore low-pass filtered with a half power point of 9 days. The correlation of P_t and P_y improved only slightly. We feel, however, that this technique is potentially very useful and with a better data set will be helpful in testing long-wave models.

e. Summary

The flow structure appears to be inviscid and baroclinic over the slope, and frictionally dominated and nonbaroclinic over the shelf. The fluctuations

TABLE 7. Correlations of terms in the momentum equations.

Position	Depth (m)	v_t, fu	v_t, P_y	fu, P_y	$(v_t + fu)$, P_y	v, P	v, P lagged†
				Phase I			
Agave	10	−0.06	−0.29*	0.21*	−0.06	−0.46*	−0.58* / −0.75 d
	29	−0.18	−0.21*	−0.21*	−0.33*	−0.34	−0.52* / −1.25 d
Sour	80	0.18	−0.41*	−0.34*	−0.48*	−0.27	−0.47* / −1.5 d
	100	−0.18	−0.33*	−0.02	−0.32*	−0.20	−0.41 / −1.25 d
Lobivia	106	0.04	−0.34*	−0.33*	−0.45*	−0.79*	−0.80* / −0.25 d
	206	−0.07	−0.43*	−0.14	−0.41*	−0.47	−0.51 / −0.75 d
	406	−0.05	0.18	0.07	0.19	−0.13	−0.30 / +1.25 d
	556	+0.08	−0.03	−0.14	−0.12	−0.27	−0.28 / +0.25 d
	626	−0.02	0.01	−0.09	−0.08	−0.13	−0.14 / +0.5 d
Islaya	41	−0.26*	−0.31*	0.29*	0.18	−0.37	−0.50* / −1.0 d
	66	−0.17	−0.35*	0.11	−0.05	−0.47*	−0.52* / −0.5 d
	116	−0.45*	−0.43*	0.05	−0.35*	−0.46*	−0.59* / −1.0 d
Mila I	28	−0.17	−0.30*	−0.13	−0.28*	−0.51*	−0.54* / −0.5 d
	53	−0.27*	−0.43*	0.08	−0.16	−0.53*	−0.62* / −0.75 d
	78	−0.27*	−0.31*	−0.07	−0.29*	−0.48*	−0.59* / −0.75 d
				Phase II			
Yuca	80	−0.10	−0.14	0.10	0.01	−0.60*	−0.61* / −0.25 d
Lagarta	115	−0.36*	−0.46*	−0.08	−0.33*	−0.75*	−0.77* / −0.5 d
	212	−0.26*	−0.18	0.11	−0.06	−0.62*	−0.62* / −0.25 d
	312	0.08	0.00	0.15	0.08	−0.23	−0.35* / +2.0 d
	412	−0.28*	−0.07	0.07	−0.04	−0.05	−0.09 / +1.0 d
Mila II	33	−0.27*	−0.45*	0.19	−0.12	−0.76*	−0.79* / −0.75 d

TABLE 7. (*Continued*)

Position	Depth (m)	v_t, fu	v_t, P_y	fu, P_y	$(v_t + fu)$, P_y	v, P	v, P lagged†
	62	−0.29*	−0.52*	0.16	−0.26	−0.70*	$\frac{-0.77*}{-0.75\ d}$
	84	−0.16	−0.53*	0.18	−0.22	−0.71*	$\frac{-0.71*}{-1.0\ d}$
	109	−0.29*	−0.52*	0.18	−0.29*	−0.74*	$\frac{-0.74*}{-1.5\ d}$
				Phase III			
Mila III	28	−0.28*	−0.55*	+0.45*	−0.12	−0.38*	$\frac{-0.52*}{-1.0\ d}$
	53	−0.33*	−0.59*	0.12	−0.42*	−0.36*	$\frac{-0.50*}{-1.25\ d}$
	79	−0.33*	−0.59*	−0.10	−0.58*	−0.27	$\frac{-0.43*}{-1.25\ d}$
	104	−0.34*	−0.60*	0.04	−0.38*	−0.13	$\frac{-0.36*}{-1.5\ d}$

* Denotes correlations significant at 95%.

† Lag time in last column is given in days (denominator). Positive values indicate that P leads v, negative otherwise.

of v in the upper part of the slope water column are strongly coupled with those on the shelf, so that even though the importance of dissipation varies spatially, the alongshore flow at depths less than about 150 m remains highly coherent. The flow on the shelf is not noticeably baroclinic until late in the experiment. It seems likely, however, that although Mila III was baroclinic in central depths, as indicated by the ϕ^{vT} results and high (v_t, fu) correlations, friction was important near the free surface and near the bottom. Over the slope, low energy levels at depth and mode structures indicate that shallow pressure gradients are compensated for by the density field below depths of about 400 m, so that, for modeling purposes, one might assume that the ocean is at rest below that depth.

5. Forcing

Earlier studies of time-dependent motion in coastal upwelling regions (e.g. Smith, 1974; Kundu and Allen, 1976; Huyer, 1976) have shown that the local component of alongshore wind stress is a primary driving mechanism for motions throughout the nearshore water column. Thus, one also expects to see high correlations between the alongshore wind stress and the fluctuations in the waters off Peru.

From the present JOINT-II observations, it appears that the local wind stress is not the only mechanism driving the motion on the slope and shelf. Table 2 shows that although the average alongshore wind stress is toward the northwest throughout the period of the study, the average alongshore component of velocity is generally in the *opposite* direction throughout the experiment. This

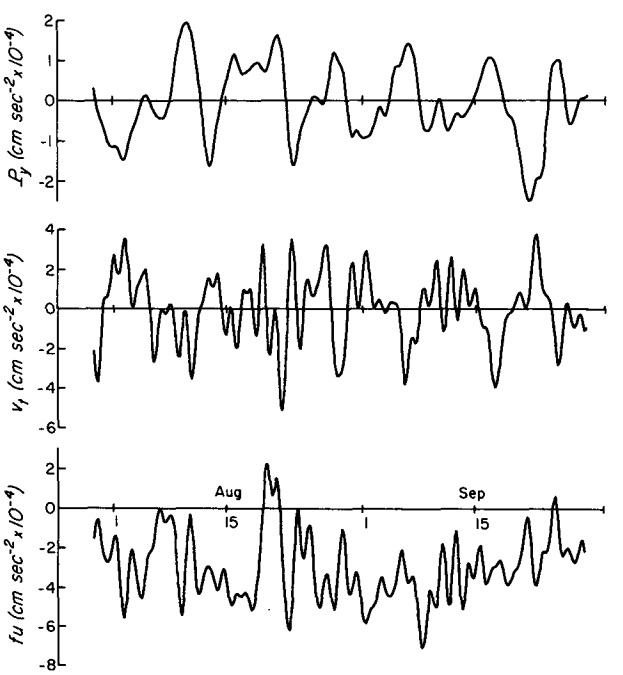

FIG. 5. P_y, v_t and fu at Mila III 53 m depth during Phase III. Note that the scale on P_y is expanded by a factor of 2.

TABLE 8. Standard deviations of terms in the momentum equations (all quantities are in cm $s^{-2} \times 10^{-4}$).

Position	Depth (m)	P_y	v_t	fu	u_t	fv	$v_t + fu$
			Phase I				
Agave	10	0.68	2.52	2.37	1.28	7.33	2.34
	29	0.68	1.89	1.38	0.86	5.05	2.07
Sour	80	0.68	1.50	1.49	0.86	5.43	2.35
	100	0.68	1.48	0.97	0.66	4.64	1.60
Lobivia	106	0.68	1.24	1.52	0.65	4.66	2.04
	206	0.68	1.17	1.26	0.46	5.72	1.65
	406	0.68	0.88	0.46	0.26	3.01	0.98
	556	0.68	0.65	0.78	0.41	1.48	1.05
	626	0.68	0.41	1.02	0.46	0.71	1.09
Islaya	41	0.68	1.24	3.29	1.18	5.03	3.15*
	66	0.68	0.97	2.11	0.86	3.96	2.17
	116	0.68	1.23	1.25	0.69	3.84	1.29
Mila	28	0.68	1.40	2.48	1.04	5.24	2.62
	53	0.68	1.03	1.84	0.97	3.58	1.86
	78	0.68	1.17	1.64	0.97	3.48	1.69
			Phase II				
Yuca	80	1.06	1.24	1.96	.94	5.00	2.22
Lagarta	115	1.06	1.32	2.69	1.10	7.51	2.53*
	212	1.06	1.16	1.11	0.64	4.46	1.38
	312	1.06	1.24	0.80	0.40	3.38	1.53
	412	1.06	0.72	0.38	0.20	1.88	0.71*
Mila II	33	1.06	2.04	2.95	1.41	9.77	3.11
	62	1.06	1.76	2.03	1.04	8.28	2.26
	84	1.06	1.71	2.04	0.88	7.22	2.45
	109	1.06	1.40	1.40	0.71	5.40	1.67
			Phase III				
Mila III	28	0.91	2.15	1.99	1.03	8.16	2.48
	53	0.91	1.74	1.69	0.88	7.11	1.98
	79	0.91	1.53	1.63	0.88	5.94	1.83
	104	0.91	1.20	1.70	0.90	4.63	1.71

* Asterisks denote cases where $SD(v_t + fu) < \max \{SD(v_t), SD(fu)\}$.

is apparently a manifestation of a countercurrent or of the Peru-Chile Undercurrent, the intensity of which may be related to the El Niño event. During the progress of the experiment, the mean (equatorward) and standard deviation of the alongshore component of wind stress in each phase increase in magnitude, and the mean (poleward) alongshore water velocity components decrease in magnitude. Thus, one expects to see the importance of the wind stress driving increase during the period of the study. One can conceptually divide the possible mechanisms for driving nearshore flows into 1) local wind driving, 2) driving by wind stress at distance along the coast, where the effects are propagated into the region of the study, 3) disturbances generated in the oceanic equatorial region which propagate eastward in the equatorial wave guide and southward along the South American Coast (Moore and Philander, 1977) and 4) driving by offshore motions.

We concentrate on discussing the results from station Mila, located on the shelf, which was maintained throughout the 1976 experiment. Comparison of the correlations of alongshore wind stress with u, v and T (Table 9) shows that the correlations increase and that the velocities and temperature come more nearly into phase with the wind stress as the experiment proceeds. Accompanying the increase in magnitude of the wind stress is a deepening of the surface mixed- or Ekman-like layer. Huyer (personal communication) documents this by means of hydrographic measurements. This is also clear from the correlations of u with the wind stress. If an equatorward wind stress is applied, the flow in the Ekman-like surface layer should be offshore, hence a negative correlation of u and τ^y should exist. The compensating flow below the surface layer should then be onshore and a positive correlation of u and τ^y should exist. The deepening can be noted by looking at the (u,τ^y) correlations at Mila. During Phase I a positive correlation exists at all Mila depths, so the mixed layer must generally be less than 28 m in depth. During the second phase, a small negative correlation exists at the shallowest meter, suggesting that the mixed-layer depth is often greater than 33 m. Finally, in Phase III a strong negative correlation exists at the shallowest meter, with a near-zero value at the next and strong positive values at greater depth. This suggests that the mixed-layer depth is often greater than 28 m, and occasionally greater than 53 m during Phase III. The secular deepening appears to be a consequence of the strengthening of the winds.

Table 3 includes the correlations at each mooring of the first two modes of u, v and T with τ^y. Again, there is secular improvement of correlations with the increasing wind stress. Of particular interest is the high correlation of the second u mode with τ^y during the last two phases, representing offshore flow in the upper part of the water column and onshore flow below in response to an equatorward wind stress. This is consistent with the accepted views of wind-driven upwelling. The second u modes suggest that during Phase II, the transient mixed-layer depth may reach about 48 m and that during Phase III about 65 m. These large depths are reasonable because of the weak stratification and the relatively small Coriolis parameter. Finally, the significant correlations of the first temperature modes with τ^y throughout the experiment suggest that, although the *alongshore* water motions may not be closely related to the local winds, temperature changes and hence effective upwelling remain linked to the local winds.

Another way to study the importance of the wind driving is to consider the mean onshore-offshore mass balance. If, in a two-dimensional case, τ^y is the sole driving mechanism for the fluid, one would expect the onshore mass flux below the surface layer to equal the wind-driven offshore surface Ekman layer mass flux $\tau^y(\rho f)^{-1}$. Table 10 presents predicted offshore and calculated onshore mass fluxes from the three phases of the experiment. As the experiment proceeded, the ratio of observed to predicted transport approached unity, suggesting that the winds gained in dynamic importance.

The question remains—what drives the frictionally dominated fluctuations on the shelf during the earlier part of the experiment? Smith (1978) has demonstrated that there are propagation effects along the continental shelf-slope system at speeds consistent with hybrid coastal trapped waves. It seems that fluctuations on the shelf, which during Phases I and II are not strongly baroclinic, may be forced by waves propagating primarily over the slope where the disturbances are baroclinic.

6. Summary

Low-frequency data from the shelf and slope regions off Peru between 12 and 15°S have been studied in an effort to understand the dynamics of the flow and its driving. Empirical orthogonal functions, correlations and physical arguments were used to obtain a picture of the flow regime.

The flow can be described as dominated by turbulent friction on the shelf (water depths $\lesssim$125 m), and as baroclinic and frictionless over the slope. The two regimes are closely coupled: the flow on the shelf with the shallower part of the strongly baroclinic flow over the slope. It appears that nonlocal driving effects are important both in

TABLE 9. Pointwise correlations of variables with alongshore wind stress (τ^y).

Position	Depth (m)	Zero-lag correlation			Maximum lagged correlation†		
		u	v	T	u	v	T
			Phase I				
Agave	10	−0.17	0.10	−0.19		0.64* −4.0 d	−0.49* +1.0 d
	29	0.40*	−0.05	0.06	0.43* +0.25 d		
Sour	80	−0.01	−0.24	0.11		−0.33* +1.0 d	
	100	−0.04	−0.13	0.27			
Lobivia	106	0.01	−0.26	0.15			
	206	−0.14	−0.32	0.19			
	406	−0.21	−0.01	0.13		−0.61* +2.25 d	
	556	0.08	0.20	−0.05		0.40* −1.0 d	−0.68* −4.25 d
	626	0.01	0.02	−0.06			−0.48* +4.75 d
Islaya	41	0.02	−0.15	0.05	−0.34* +3.75 d		0.42* +4.75 d
	66	0.26	−0.10	0.07			0.40 +3.0 d
	116	0.10	−0.16	0.37			0.50* +1.5 d
Mila	28	0.17	−0.11	−0.15	0.36 +2.25 d	0.34* +3.75 d	
	53	0.40*	−0.23	0.23	0.47* +1.75 d		0.51* +3.25 d
	78	0.27*	−0.28	0.13	0.33* +0.5 d		0.37 +3.5 d

TABLE 9. (*Continued*)

Position	Depth (m)	Zero-lag correlation			Maximum lagged correlation†		
		u	v	T	u	v	T
			Phase II				
Yuca	80	0.28*	0.21	−0.07		−0.43* +5.0 d	−0.41* +3.5 d
Lagarta	115	0.22	0.11	0.00	0.31* +0.75 d		−0.39* ⩾ +3.5 d
	212	0.01	0.32	−0.22		0.33* +0.25 d	−0.36* +1.0 d
	312	0.00	0.16	−0.15			−0.34* +1.5 d
	412	0.05	0.23	−0.07			−0.33 +1.75 d
Mila II	33	−0.27*	0.26	0.06	0.34* −2.0 d	0.33* +1.25 d	0.41* −2.0 d
	62	0.24	0.23	0.03		0.30* +1.0 d	0.37* −2.25 d
	84	0.55*	0.19	−0.07	0.57* +0.25 d		−0.41* +2.25 d
	109	0.44*	0.21	−0.10	0.45* −0.25 d		−0.33* +1.75 d
			Phase III				
Mila III	28	−0.49*	0.50*	−0.32	−0.51* +0.25 d	0.51* +0.25 d	−0.66* +1.5 d
	53	0.08	0.44*	−0.43*		0.46* +0.5 d	−0.66* +0.25 d
	79	0.57*	0.39*	−0.51*	0.57* 0.0 d	0.40* +0.5 d	−0.71* +1.0 d
	104	0.53*	0.35*	−0.55*	0.53* 0.0 d	−0.31* +2.25 d	−0.73* +1.0 d

* Denotes correlation significant at 95%.

† All maximum lagged correlations less than 0.30 are deleted, and those not significant at 95% where u, v, or T leads τ^v are deleted as meaningless. Those where u, v, T lead are denoted by a negative lag time (days).

the mean flow, which is opposite to the local wind, and in the fluctuations, which Smith (1978) has shown to have a component propagating from the north. This picture does change somewhat over the six months of the experiment as the local winds increase in magnitude. The depth of the turbulent bottom layer decreases by about a factor of 2, but remains large. The effect of the local wind driving increases in time, as evidenced by the growing correlations and decreasing phase lags between the alongshore wind stress and the velocity components. As the frictional effects on the shelf decrease, the baroclinic structure becomes more pronounced.

TABLE 10. Time-averaged onshore subsurface transports.

	$\bar{\tau}^v (\rho f)^{-1}$ (cm² s⁻¹ × 10⁴)	Observed transport (cm² s⁻¹ × 10⁴)	Ratio of observed to predicted transport
Islaya	2.2 ± 0.3	4.5 ± 2.1	2.0 ± 1.3
Mila I	2.2 ± 0.3	4.7 ± 1.4	2.1 ± 1.0
Mila II	2.3 ± 0.3	4.0 ± 1.8	1.7 ± 1.0
Mila III	2.8 ± 0.3	4.1 ± 1.2	1.5 ± 0.6

A temperature increase during Phases I and II is related to the strong southeastward mean flow in the upper part of the water column. This temperature increase, apparently associated with the El Niño event, somewhat masks the upwelling driven

by the local winds throughout the experiment. Nevertheless, it seems that an upwelling circulation existed throughout the experiment, as shown by the significant correlations on the shelf of temperature and the alongshore wind stress. Momentum balances in the upper part of the water column were strongly three-dimensional, although the mean mass balance on the shelf becomes nearly two-dimensional.

Acknowledgments. This research was supported by the Coastal Upwelling Ecosystems Analysis program (CUEA) of the International Decade of Ocean Exploration Office (IDOE) of the National Science Foundation under Grants OCE-76-00596, OCE-78-03380, OCE-76-00132 and OCE-03382 and also (for J. S. Allen) partially by the Oceanography Section, National Science Foundation, under Grant DES-75-15202.

REFERENCES

Allen, J. S., 1975: Coastal trapped waves in a stratified ocean. *J. Phys. Oceanogr.*, **5**, 300–325.

——, 1976: Continental shelf waves and alongshore variations in bottom topography and coastline. *J. Phys. Oceanogr.*, **6**, 864–878.

——, and P. K. Kundu, 1978: On the momentum, vorticity and mass balance off the Oregon coast. *J. Phys. Oceanogr.*, **8**, 13–27.

Barton, E. D., 1977: JOINT-II—R/V *Thomas G. Thompson* cruise 108 Leg I CTD measurements off the coast of Peru near Cabo Nazca, April-May 1976. CUEA Data Rep. 39, 140 pp.

Brink, K. H., and J. S. Allen, 1978: On the effect of bottom friction on barotropic motion over a continental shelf. *J. Phys. Oceanogr.*, **8**, 919–922.

Clarke, A. J., 1977: Observation and numerical evidence for wind-forced coastal trapped long waves. *J. Phys. Oceanogr.*, **7**, 231–247.

Davis, R. E., 1976: Predictability of sea surface temperature and sea level pressure anomalies over the North Pacific Ocean. *J. Phys. Oceanogr.*, **6**, 249–266.

Gunther, E. R., 1936: A report on oceanographical investigations in the Peru coastal currents. *Discovery Rep.*, **13**, 107–276.

Halpern, D., 1976: Structure of a coastal upwelling event observed off Oregon during July 1973. *Deep-Sea Res.*, **23**, 495–508.

Huyer, A., 1976: A comparison of upwelling events in two locations: Oregon and Northwest Africa. *J. Mar. Res.*, **34**, 531–546.

——, B. M. Hickey, J. D. Smith, R. L. Smith and R. D. Pillsbury, 1975: Alongshore coherence at low frequencies in currents observed over the continental shelf off Oregon and Washington. *J. Geophys. Res.*, **80**, 3495–3505.

Kundu, P. K., 1977: On the importance of friction in two typical continental waters: off Oregon and Spanish Sahara. *Bottom Turbulence*, J. C. J. Nihoud, Ed., *Proc. 8th Liège Colloquium on Ocean Hydrodynamics* (1976), 187–207.

——, and J. S. Allen, 1976: Some three-dimensional characteristics of low frequency current fluctuations near the Oregon Coast. *J. Phys. Oceanogr.*, **6**, 181–199.

——, ——, and R. L. Smith, 1975: Modal decomposition of the velocity field near the Oregon Coast. *J. Phys. Oceanogr.*, **5**, 683–704.

Mittelstaedt, E., R. D. Pillsbury, and R. L. Smith, 1975: Flow patterns in the Northwest African upwelling area. *Dtsch. Hydrogr. Z.*, **28**, 145–167.

Mooers, C. N. K. and R. L. Smith, 1968: Continental shelf waves off Oregon. *J. Geophys. Res.*, **73**, 549–557.

Moore, D. W. and S. G. H. Philander, 1977: Modeling of the tropical oceanic circulation. *The Sea*, Vol. 6, Part 1, Wiley, Chap. 8.

Smith, R. L., 1974: A description of current, wind, and sea level variations during coastal upwelling off the Oregon coast, July–August 1972. *J. Geophys. Res.*, **79**, 435–443.

Smith, Robert L., 1978: Poleward propagatinig perturbations in currents and sea level along the Peru coast. *J. Geophys. Res.* (in press).

——, D. B. Enfield, T. S. Hopkins and R. D. Pillsbury, 1971: The circulation in an upwelling ecosystem: The *Pisco* cruise. *Inv. Pesq.*, **35**, 9–24.

Wang, D-P., and C. N. K. Mooers, 1976: Coastal-trapped waves in a continuously stratified ocean. *J. Phys. Oceanogr.*, **6**, 853–863.

——, and J. J. Walsh, 1976: Objective analysis of the upwelling ecosystem off Baja California. *J. Mar. Res.*, **34**, 43–60.

Wimbush, M., and W. Munk, 1970: The benthic boundary layer. *The Sea*, Vol. 4, Part 1, Wiley, Chap. 19.

Wyrtki, K., 1963: The horizontal and vertical field of motion in the Peru current. *Bull. Scripps Inst. Oceanogr.*, **8**, 313–346.

——, 1964: The thermal structure of the Eastern Pacific Ocean. *Dtsch. Hydrogr. Z., Erganzungsh.*, **A6**, 84 pp.

Wyrtki, K., 1977: Advection in the Peru current as observed by satellite. *J. Geophys. Res.*, **82**, 3939–3943.

Zuta, S., and W. Urquizo, 1972: Temperatura promedio de la superificie del mar frente a la costa Peruana, periodo 1928–1969. *Bol. Inst. Mar. Peru*, **2**, 459–520.

——, T. Rivera and A. Bustamante, 1975: Hydrological aspects of the main upwelling areas off Peru. Paper presented at the Third International Symposium on Upwelling Ecosystems, University of Kiel.